Part 1

Guidselines for Book Preparation in MS Word using WSPC Style

Chapter 1

In-silico Finite Element wear predictions

1.1 Introduction

Finite Element (FE) models can be considered a gold standard in mechanical design as well as in many other fields. In the last decades, the complexity of models and simulations has rapidly increased, taking advantage of improvements in software and technologies.

Wear modeling involves many aspects also at different scales, from micro to macrogeometries. A general overview of the problem is described in Chapter [], where a simple analytical approach is presented, which is useful for a first approximation of the solution when the contact problem can be solved analytically and the geometry modification due to wear is negligible. In a more general case, in particular in non conformal contacts, it is important to estimate the evolution of the contact pressure and surface geometry as wear progresses. That can be conveniently investigated by FE models, using predefined tools or user-subroutines.

In this Chapter the main points of FE wear simulations are discussed with some examples, first examining steady state boundary conditions (BCs) and secondly cyclic loadings. The major limit of these analyses is their computational cost which can be reduced by the application of the submodeling technique, introduced in the last part of the chapter.

1.1 FE Wear models: general aspects

When adopting a Finite Element approach, the main steps of wear simulations include (Fig. 1.1):

a. contact analysis, to determine the contact pressure and the sliding distance between the surfaces in contact;

b. wear calculation, for each node the increment of wear depth is calculated according to the adopted wear law, most frequently the Archard wear law. This step can be performed through an automatic software tool or through a user defined routine, e.g. the UMESHMOTION in Abaqus®;

c. wear implementation and mesh smoothing; the calculated wear depth is applied to the mesh as a displacement of the nodes, so that geometry is modified. In order to avoid excessive elements distortion or collapse, a check on their shape is performed and, if needed, the mesh is improved with an adaptive mesh smoothing.

These steps are repeated iteratively to simulate a loading history, i.e. a specific operational time of the component. Thus, a complete simulation can require hours or days. As already stressed, the computational cost remains the main drawback of wear FE analyses [1-4], therefore analysis settings should be accurately chosen to achieve reliable results in a reasonable time.

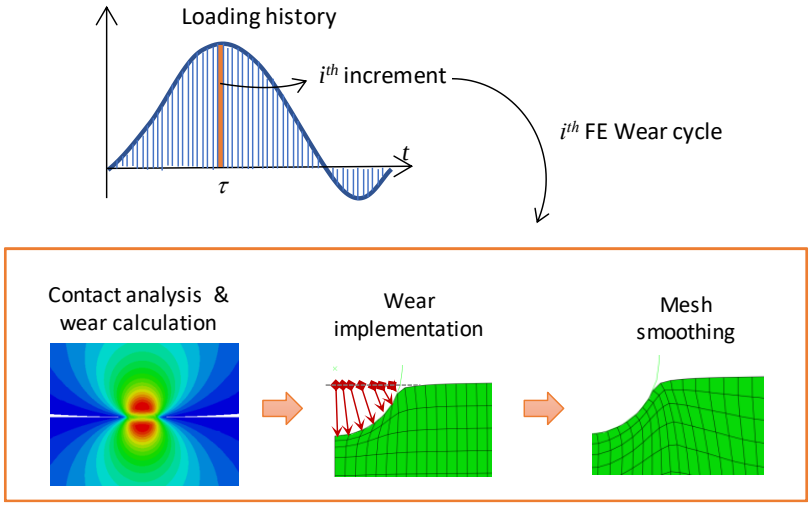

Fig. 1.1. Basic steps in wear simulations of generic loading history. (Adapted and reprinted from [4] with permission from Elsevier).

1.1.1 *Wear calculation*

As mentioned above, wear calculation can be performed through a specific tool of the FE software or by user defined routines called by the software itself. That depends both on the software and the adopted wear law (see Chapter [], Sec.1.3). For example, in Ansys® APDL and Workbench the generalized Archard law is predefined; accordingly, the wear depth increment Δh occurring during the time interval Δt is evaluated as

$$\Delta h = \frac{K}{H}\, p^m |\, \boldsymbol{v}_s|^n\, \Delta t \tag{1.1}$$

where K is the wear factor, H the material hardness, p the contact pressure, $\boldsymbol{v}_s$ the sliding velocity so that $|\, \boldsymbol{v}_s|\, \Delta t$ represents the sliding distance.
On the other hand, the implementation of more complex wear laws, as those based on the cross-shear described in Chapter [], typically requires user defined subroutines, with properly defined input (e.g. stress and strain fields, sliding distance increment components) and wear increment and direction as output. This option is available, for example, both in Ansys® and in Abaqus®.
In user subroutines, the discrete form of the wear increment at the node k at a given iteration i, is expressed using the average pressure between two consecutive time steps and the sliding increment Δs i.e.

$$\Delta h_i^k = \frac{K}{H}\left(\frac{p_i^k + p_{i-1}^k}{2}\right)^m \left(\frac{s_i^k - s_{i-1}^k}{\Delta t}\right)^n \Delta t \tag{1.2}$$

Sometimes the average pressure is replaced by the actual pressure value.

1.1.1.1 *Implicit or explicit kinematics*

In general, the sliding distance/velocity at each node is calculated during the simulation, specifying the relative motion of the contact bodies as a boundary condition. This is sometimes referred to as explicit kinematic approach. As an example, consider the pin-on-plate wear test shown in Fig. 1.2. The pin can only translate towards the plate under the action of the load $\boldsymbol{F}$, while the plate translates horizontally, specifying its position

in the fixed frame at each time step. That implies that the meshes of the contact surfaces in general have nodes differently misplaced at each time step, that can produce some minor 'irregularities' in contact pressure profile.

However, in some particular cases, i.e. when the relative motion is translatory, the contact is frictionless and only one body (the pin in the example) gets worn, the alternative implicit kinematics formulation can be adopted.

This consists in combining a static analysis and a modified wear law with a fictitious wear coefficient k^*, i.e.

$$\Delta h = k^* \, p^m \, \Delta t \quad \text{with} \quad k^* = \frac{K}{H} \, |\boldsymbol{v}_s|^n \tag{1.3}$$

For the case of the pin-on-plate, simulations can be performed also fixing the plate in a static configuration and calculating wear through the modified law of Eq.(1.3).

To note that the implicit kinematic formulation is very useful for reducing computational costs in case of long sliding distance to be simulated.

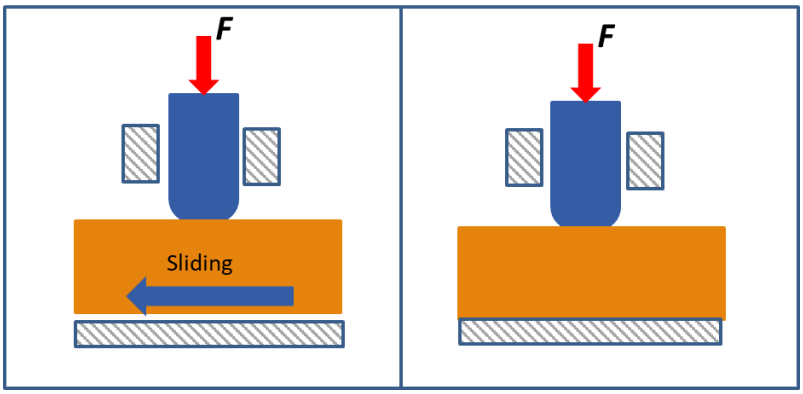

(a) (b)

Fig. 1.2. Pin on plate scheme with explicit (a) or implicit (b) kinematic approach.

1.1.1.2 *Unilateral or bilateral wear*

In wear simulations, a distinction is usually made between two cases: unilateral or asymmetric wear, when only one body undergoes wear, bilateral or symmetric wear when both bodies get worn (Chapter [], Sec. 1.3.1). The distinction depends on the wear resistance of the rubbing surfaces. In many cases, e.g. brakes, it is a design choice to have only one element subjected to wear, but in other cases, e.g. gears, wear is bilateral.
In numerical simulations, bilateral wear is somehow more complex, often solved as a combination of two unilateral cases, simulating a double contact. That also implies an increase of the computational time.
Another point should be mentioned about bilateral wear: for each surface of the coupling, a wear law is required. In case of the Archard wear law, it means $k=K/H$ for each material. However, since wear is a phenomenon characterizing the coupling itself, such values cannot be used as specific of each material and applied in different conditions, but remain defined for the test case used to evaluate them. This is an important limitation since separate indications for the coupling elements are rare [1, 2, 4]. Often the total volume loss is measured and a simple equi-ripartition is supposed, meaning the same K/H value is adopted for both materials [1].

1.1.2 *Mesh definition*

When defining the mesh of a wear model, the same indications used for the contact analysis hold. The element size should be properly selected considering the characteristic dimension of the contact area, that means having very small elements for non conformal contacts. However, two points are worth remembering, as furtherly detailed in Sec.1.3:

a) Wear increases the conformity of the contact surfaces, causing an increment of the contact area, with a consequent reduction of contact pressure. Thus, a coarse mesh that initially approximates the pressure distribution could be good to catch its evolution with wear.
b) Mesh smoothing settings are usually based on the reduction of the element volume with time, as wear proceeds. For example, assuming that the threshold is a 50% volume reduction, small elements require mesh smoothing more often than larger elements,

that means also longer computational times. Thus, a good compromise is fundamental when choosing the elements size in wear models.

1.1.3 *Model validation*

Model validation is a crucial point in all the applications. A comparison with reliable experimental results should be performed to assess the accuracy of the simulations. As already stressed in Chapter [], wear models are usually validated considering only the wear volume, but also the wear map is fundamental. The reason is double: on the one hand the volume loss is used to evaluate *K/H*, on the other hand the same wear volume can be produced by different wear maps. Consequently, only wear map validation would confirm the reliability of both the model and the wear law adopted to describe the phenomenon.
However, since wear is a very complex phenomenon, dependent on many factors, wear test results usually have a wide dispersion. Therefore, one should not aim at a 'perfect' correlation of numerical and experimental predictions but should be satisfied of a good agreement in the range of the experimental dispersion.

1.2 Simulation of cyclic conditions

1.2.1 *General procedure*

In many applications, wear is caused by periodic loading conditions, such as in pin-on-plate sliding tests or gait cycle wear tests for hip prostheses. Consequently, experimental and numerical wear investigations typically need to simulate of a very high number of wear cycles, e.g. up to 5 Mc (million cycles) for wear in hip prosthesis.
FE wear simulations of cyclic conditions performing a quasi-continuous geometry update could have a very high computational cost. As schematic example, consider a periodic loading history characterized by N loading cycles, shown at the top of Fig. 1.3. Assuming each wear cycle discretized in n_c increments, the simulation of the whole loading history would require

a number n=N n_c of contact analyses (i.e. FE runs) and geometry updates (i.e. FE wear cycles). This means that, for instance, in case of FE wear cycles discretized in 25 increments each one processed in 30 s, the simulation of 1000 cycles would last about 9 days. That points out the key role of simplifying hypotheses and computational strategies in reducing the duration of wear simulations. For this purpose, the accelerated update procedure illustrated at the bottom of Fig. 1.3 has been demonstrated to be very effective [2, 4-8]. Basically, it hypothesizes that wear affects the contact pressure only after a critical number $\overline{N}$ of cycles because the wear depth in a wear cycle is usually very low. Consequently, the geometry update can be performed every $\overline{N}$ cycles, allowing to extremely accelerate the wear simulation that needs a lower number $n_u = N/\overline{N}$ of FE wear cycles, and a lower number $n = n_u\, n_c$ of FE runs. In fact, the parameter $\overline{N}$ is also known as accelerated factor [5]. Accordingly, for each wear cycle u (Fig. 1.3), the local wear depth at the node k accumulated during a given wear cycle u is calculated by applying the accelerated factor $\overline{N}$ as it follows, assuming the Archard wear law:

$$\Delta h_u^{\kappa} = k\,\overline{N} \sum_{i=1}^{n_c} \frac{\left(p_{u,i}^{\kappa} + p_{u,i-1}^{\kappa}\right)}{2} \left(s_{u,i}^{\kappa} - s_{u,i-1}^{\kappa}\right) \tag{1.4}$$

where i is the generic increment within the wear cycle. It is worth noting that although $\overline{N}$ is typically considered constant during wear evolution, it strongly depends on the simulated tribological conditions. Moreover, the correct setting of both $\overline{N}$ and n_c needs a critical sensitivity analysis [4].

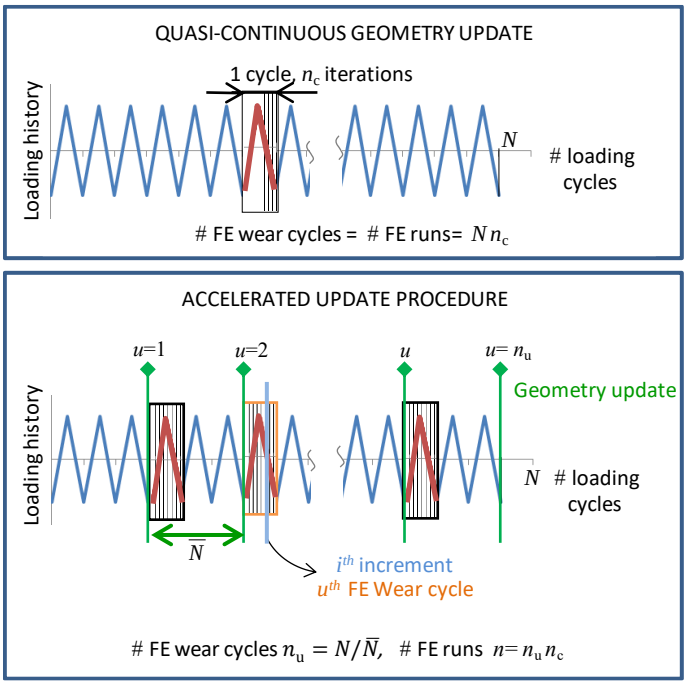

Fig. 1.3. Procedures for wear simulations under cyclic conditions: quasi continuous vs. accelerated geometry update procedure (Adapted and reprinted from [4] with permission from Elsevier).

1.2.2 *Application to cylinder-on-plate reciprocating wear tests*

This section provides an example of the application of the accelerated procedure presented by the authors in [4]. The case study consists in a cylinder-on-plate under reciprocating contact, with the rubbing surfaces having different wear resistances, as shown in Fig. 1.4(a). This relatively simple model was exploited to investigate:

a) Model converge criticality for the accelerated procedure;
b) The evolution of the contact and wear parameters during wear progress;

c) The effect of the partition factor α (Eq.(1.5) in Chapter []), i.e. wear redistribution, on wear parameters;
d) The effect of the stroke amplitude s_t, on wear parameters.

1.2.2.1 *Model description*

A 2D (plane strain) wear model was developed in Abaqus® using the UMESHMOTION subroutine, ad-hoc coded in FORTRAN.
The model consists in a cylindrical pin of radius R=10 mm coupled with a plate of length 2R, both made of metal. The non conformal contact is assumed to be frictionless and is set as double, allowing the simulation of bilateral wear. The cyclic loading conditions consist in reciprocating sliding contact under a constant load of 100 N. As shown in Fig. 1.4(b), the top surface of the pin is built in, whilst the kinematics of the plate is driven by the reference point (*RP*) of a rigid base tied to bottom of the plate so that rotation is constrained, y translation is controlled by the load applied to the rigid base, and x translation is used to reproduce the reciprocating contact, as described in Fig. 1.4(c). Consequently, an explicit kinematics formulation is adopted. In particular, both fretting (reciprocating motion) and sliding wear (half-reciprocating motion) are simulated by varying the stroke amplitude s_t, for a total of 4 conditions: $s_t=a$, $s_t=2a$, $s_t=4a$, $s_t=R$, where a=0.11 mm is the hertzian semi-width in unworn status.
Although contact bodies are both metallic, different wear resistances of the rubber surfaces are simulated assuming α values of 0 (no wear of pin), 0.25, 0.5, 0.75, 1 (no wear of plate), and the same couple wear coefficient $k=10^{-8}$ mm^2/N.

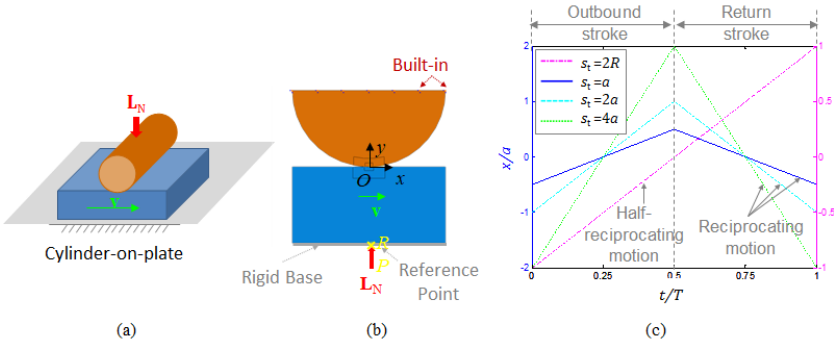

Fig. 1.4. Modeling of cylinder-on-plate wear tests (a, b) under cyclic conditions characterized by periodic reciprocating sliding contact under a constant load (stroke amplitude, s_t ; Hertzian semi-width a) (c). (Adapted and reprinted from [4] with permission from Elsevier).

1.2.2.1 *Results*

a) Model convergence analysis

The convergence analysis of wear models assuming the accelerated procedure is very critical. It has a double face, as it must be performed both for the unworn configuration, i.e. classical mesh sensitivity analysis, and the worn configuration, i.e. setting of $\overline{N}$ and n_c.To note that, a too high $\overline{N}$ or a too low n_c, could cause numerical instabilities such as local peaks of contact pressure and unsmooth worn surfaces, whilst, the contrary could slow down the simulations. Consequently, once the mesh for the unworn condition is defined, the sensitivity analysis on $\overline{N}$ and n_c allows to identify values that guarantee a good compromise between accurate results and computational cost.

Figure 1.5 shows some results of the convergence analysis for the cylinder on plate model, for the case s_t=a and α=0.5 [4]: the contact pressure distribution (Fig. 1.5(a-c)) and the plate wear profiles (Fig. 1.5(d)) are compared for different combinations of $\overline{N}$ and n_c values. Low values of n_c (<100) causes local contact peaks, independently on $\overline{N}$ values, whilst, high values of n_c (≥100) can produce smooth and symmetric contact pressure profiles when combined with quite high $\overline{N}$ values ($\overline{N}$≥100). To

note that lateral peaks are expected as caused by discontinuities in curvature radius at the contact edges. Low values of n_c also cause unsmooth and asymmetric wear profiles, as shown for the plate in Fig. 1.5 (d). According to the convergence analysis, the combination n_c=100 and $\bar{N}$=100 guarantees both smooth contact pressure and wear profiles, as shown at the bottom of Fig. 1. 5.

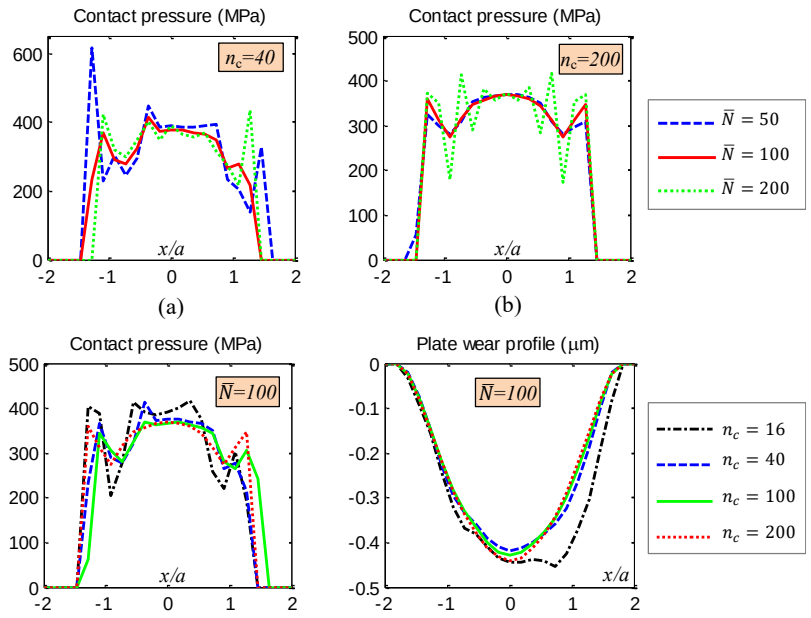

Fig. 1.5. Model convergence analysis for simulations of cyclic conditions: effect of of $\bar{N}$ and n_c on numerical instabilities in the prediction of the contact pressure (a-c) and the worn profiles (d) obtained for s_t=a and α=0.5, at N=1000 (Adapted and reprinted from [4] with permission from Elsevier).

b) Evolution of contact and wear parameters

The typical results of a FE wear model consist in the evolution of contact pressure and wear profiles during the loading history. An example is provided in Fig. 1.6 for the case s_t=a and α=0.5. In unworn conditions (i.e. at the first load cycle) the contact is described by the Hertzian theory. Later, as the surfaces wear out, the contact becomes more conformal: a

wear scar develops on the pin surface while a wear groove hollows the plate surface out, the contact area widens, and the contact pressure flattens. The contact pressure at the centre of the worn area, referred to as maximum contact pressure, decreased rapidly in the first 1000 wear cycles. This trend is reflected in the evolution of the maximum wear depth of both pin and plate surfaces, which increase faster in the first phase of the wear process. On the contrary, in agreement with the theory, the trends of wear volumes (single body and couple) are linear and in particular, being α=0.5, equal wear volumes are predicted for pin and plate.

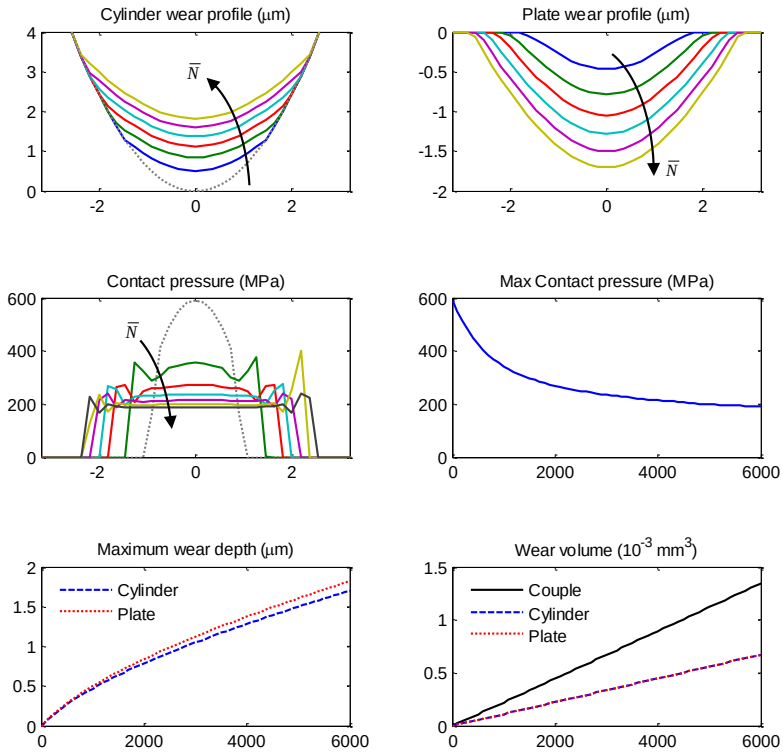

Fig. 1.6. Evolution of contact and wear parameters for the case s_t=a and α=0.5, over 6000 wear cycles (Adapted and reprinted from [4] with permission from Elsevier).

c) Effect of the wear partition factor

As largely discussed in Chapter [], the different wear resistance of the rubbing surfaces, though rarely discussed and modelled in literature, is a key aspect of the wear process.

The pin-cylinder model is used to demonstrate the important effect of the partition factor on wear evolution, by assuming α values in the range 0-1. Both unilateral (α= 0, 1) and bilateral (α= *0.25, 0.5, 0.75*) wear conditions are considered.

Moving from the case of unilateral wear of pin (α= 0) to unilateral wear of plate (α= 1), the higher the α value, the more marked and wider the pin scar and the less deep the plate grove, as also confirmed by the evolution of the maximum wear depth of the coupled bodies. Moreover, as α increases, the contact gets more conformal: the contact area increases and the contact pressure flattens, and its maximum value drops down rapidly during wear evolution. However, it should be noted that the effect of α on the contact pressure is more important for higher stroke amplitude ($4a$ vs a). By varying the value of α, the contact pressure distributions are very similar for $s_t=a$ whilst much different for $s_t=4a$, moving from a quasi-hertzian profile at α =0, to a flatten profile for α=1. This is also reflected on the evolution of the maximum contact pressure which, in case of $s_t=4a$, changes significantly passing from a linear (α =0) to a faster and strongly non linear (α =1) decrease.

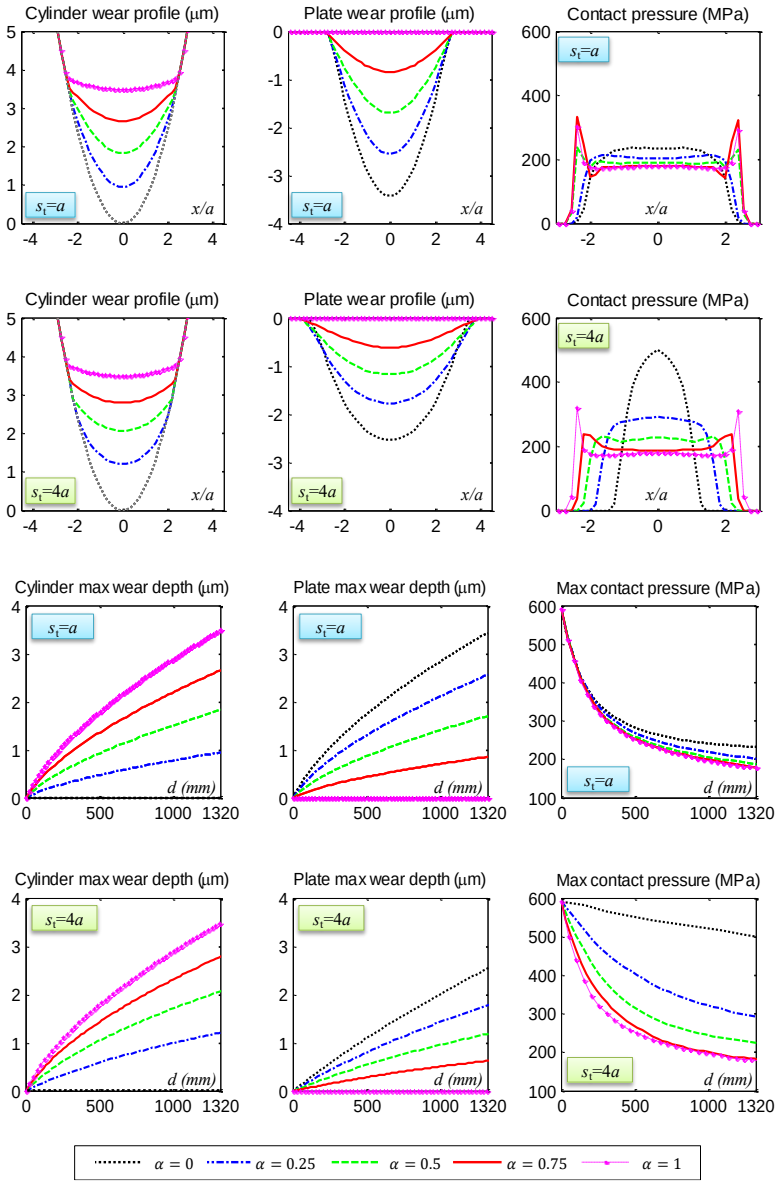

Fig. 1.7. Effect of the wear partition factor α on cylinder and plate wear profiles and contact pressure (for a sliding distance of 1320 mm) and the evolution of maximum wear depth and contact pressure. (Adapted and reprinted from [4] with permission from Elsevier).

d) Effect of the stroke amplitude

The simulation of different stroke amplitudes allows to investigate much different wear conditions, such as the fretting (s_t=a, 2a, 4a) and the sliding wear (s_t=2R). Also in this case, results are presented in terms of wear and contact pressure profiles, for different values of α, as shown in Fig. 1.8. The effect of the kinematic conditions is certainly important, though variable with α. In case of bilateral wear or unilateral wear of pin (first two rows), the effect of s_t is comparable to that one of α: the higher s_t, the less deep the plate groove and thus less conformal the contact, with higher contact pressures (less flatten). However, it should be noted that the effect of s_t on the contact pressure profile is more marked for higher values of α (i.e. 0.5 vs 0). On the other hand, in the extreme case of unilateral wear of the pin (α=1), the effect of s_t is negligible both on the wear profile and the contact pressure. Results demonstrate that fretting and sliding wear cause much different wear damage, with maximum contact pressure higher and potentially more dangerous in the latter case.

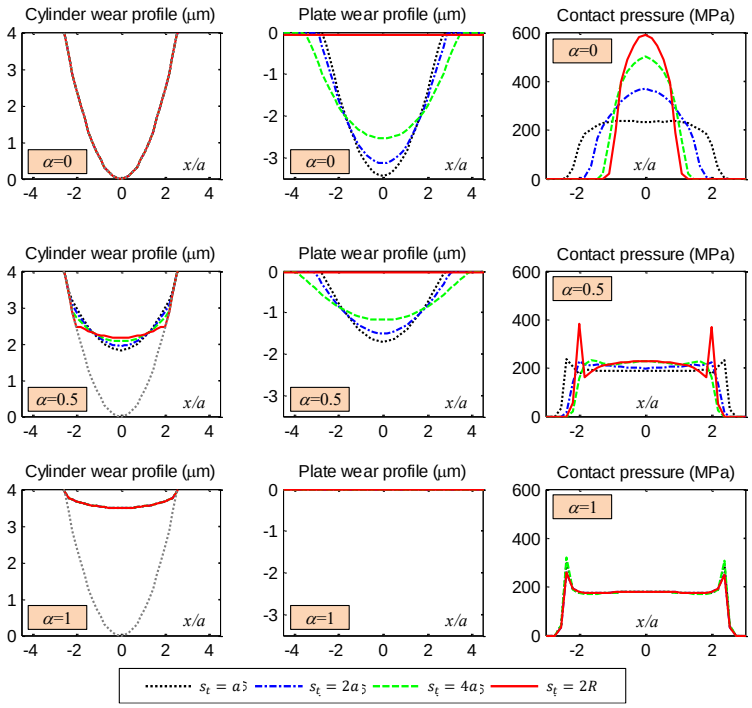

Fig. 1.8. Effect of the stroke amplitude s_t on wear profiles (cylinder in left column, pin in central column) and contact pressure (right column) for a sliding distance of 1320 mm. Specific wear partition factor α are considered in each row (Adapted and reprinted from [4] with permission from Elsevier).

1.3 Application of the submodeling technique

1.3.1 *General aspects and procedure description*

The submodeling technique is one of the methods that can be used to reduce the computational cost problem of FE wear simulations. Compared to other strategies proposed to minimize the calculation time, mainly based on extrapolation methods [9, 10], this technique proved to be an efficient solution also when few loading cycles are considered [3].

The main idea behind the submodeling approach for generic FE models is that the solution of a coarse-mesh-model of the entire system, usually called *global* model, can be used to provide the boundary conditions to a fine-mesh-model (submodel or *local* model*)* that only includes the region of interest (RoI). Nodal displacements, forces or stresses are usually extracted from the global model solution at the cut-boundaries and then applied to the local model (Fig. 1.9). The solution obtained using the combination of global and local model is accurate and usually faster than the one achieved with the entire detailed model.

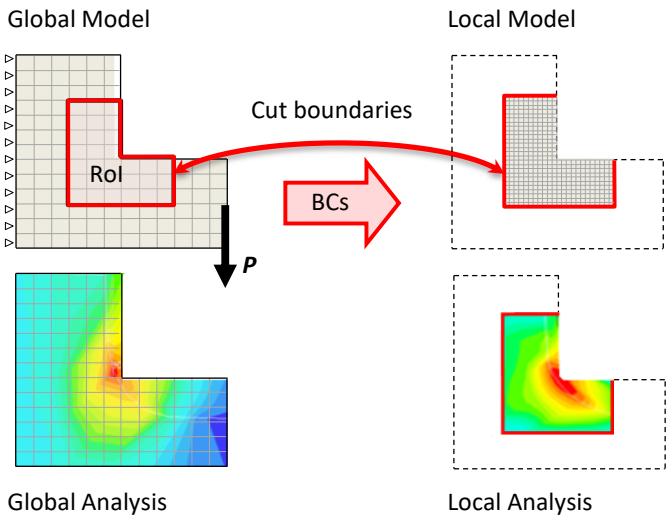

Fig. 1.9. Submodeling in FE analysis. The solution of the coarse global model is used to provide the BCs to a fine local model that includes the RoI delimited by the cut boundaries. The accuracy of the results is improved in the local model. (Reprinted from [3] with permission from Elsevier).

When applying the submodeling technique to wear models, the general workflow depicted in Fig. 1.10 can be adopted [3]. Three main important steps can be identified: development of the global model, development of the local model and wear simulations.

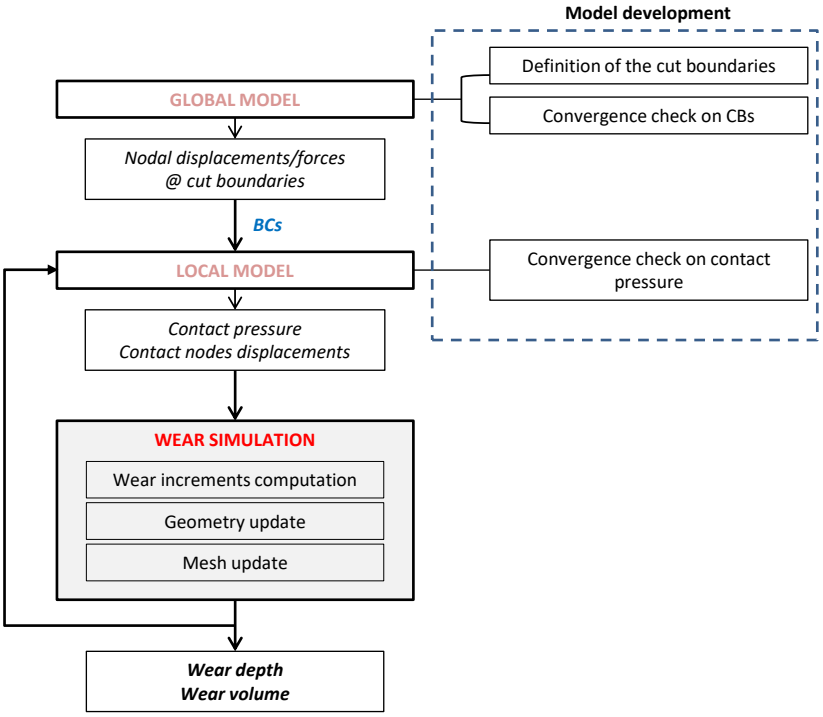

Fig. 1.10. Main steps of the FE wear submodeling procedure: a) global model development, b) local model development and c) wear simulations. (Reprinted from [3] with permission from Elsevier).

a) Global model development

The global model is solved to provide the boundary conditions to the local model used to simulate the wear test. Two important aspects of the global model development should be careful evaluated. The first one regards the definition of the cut-boundaries. Submodeling is based on the St. Venant's principle and general recommendations suggest placing the cut-boundaries far enough away from the stress concentration region. In case of wear analyses, this region varies during the simulation because the contact area increases do to wear. The cut-boundaries should be

thus defined so that they can be considered far enough away from the stress concentration region for the entire wear simulation. The second important aspect for global model development is related to the 'acceptable' mesh density. Despite contact pressure is usually not an output of this model and can be roughly estimated using a coarse mesh, a converge analysis on the quantities to be transferred (i.e., nodal forces, displacements or stresses at the interfaces) is needed in order to reduce the so called 'boundary conditions error' [11]. The element size at the contact region of the global model should be thus properly selected so that the 'right' behaviour at the interfaces of the system is captured.

b) *Local model development*
The first critical step of this model development phase is the definition of the boundary conditions. The most common submodeling approach in structural mechanics is based on the use of nodal displacements. However, this strategy cannot be purely applied for wear analyses because the geometry significantly changes after the material removal. Alternative stress and force-based techniques can be evaluated, eventually combined with the displacement-based one in a hybrid scheme. Choosing the right mesh density to accurately predict contact stresses and wear is a second important aspect in the local model development. A mesh convergence analysis aimed at reducing the discretization error on the maximum contact pressure is proposed in the wear submodeling procedure. However, general considerations on the effect of the element size on the wear simulation results (Sec 1.3.2.2) should be taken into account in this phase.

c) *Wear simulations*
The main steps of wear simulations (Sec. 1.1.1) are usually performed entirely with the local model while the global model is used to simulate a simple contact analysis in the initial unworn configuration. This is the case of the single point contact example that will be presented in the following section and used to discuss the validity of the wear submodeling procedure. However, it is

worth noting that in case of more complex wear problems (e.g., multipoint contact and wear analyses where the total contact force acting on the contact surfaces might change during the first simulation phase as a result of different contact geometries), also the global model can be used to simulate the first wear cycles in order to correctly estimate the boundary conditions at the model interfaces.

The general wear submodeling procedure is here described in its simplest formulation. In fact, the global model is used only for the initial unworn configuration and the boundary conditions are transferred to the local model and kept constant for the entire wear test. To remember the important assumption that the boundary conditions at the selected interfaces do not vary significantly with wear/time since the cut boundaries are set far enough away from the stress concentration region for the entire wear simulation. However, in general, the consistency of this assumption should be always checked. To this aim, contact analyses performed on the global modal with reasonably expected wear profile might help in defining the cut boundaries and assess model assumption. On the other hand, for the cases where BCs at the cut boundaries evolves with wear, new global analyses with the updated worn geometry are needed, thus performing global-local model iterations.

1.3.2 *Validation of the submodeling procedure*

In this section, the validity of the wear submodeling procedure is discussed for the case of a single point contact. In particular, the case study presented in [3] is considered, which consists in a pin-on-disc wear test where a metal hemispherical head pin is in contact with a metal rotating disc under a constant normal load (Fig. 1.10).

1.3.2.1 *Models description*

Two-dimensional axisymmetric models were developed in Ansys® mechanical APDL. The global model consisted in a quarter of circle of radius R and a quadrilateral region of dimension $R \times R$, with R=5 mm. A

constant load of 21 N is applied at a reference node at the bottom rigid surface of the disc while the top surface of the pin is built in (Fig. 1.10).
The local model consists in the subregions introduced in the global model and delimited by the cut boundaries of length w=1 mm (about 10 times the Hertzian contact half-width, a, in the unworn condition). A hybrid submodeling approach is adopted where nodal forces and displacements extracted from the global model solution, are mapped respectively to the disc and pin boundaries. The wear test is simulated using the local model for a total sliding distance of 3 m.
For both global and local models, the contact is simplified as frictionless and the material loss is attributed only to the pin. The kinematics is implicitly modeled by introducing a fictitious wear coefficient $k^*= k\ v$, where k is the wear coefficient set to 1.25×10^{-13} Pa^{-1} and v is the sliding velocity, assumed uniform in the contact nodes and equal to 25 mm/s. The wear model was implemented in the software using the TBDATA,WEAR command with the Archard law option.

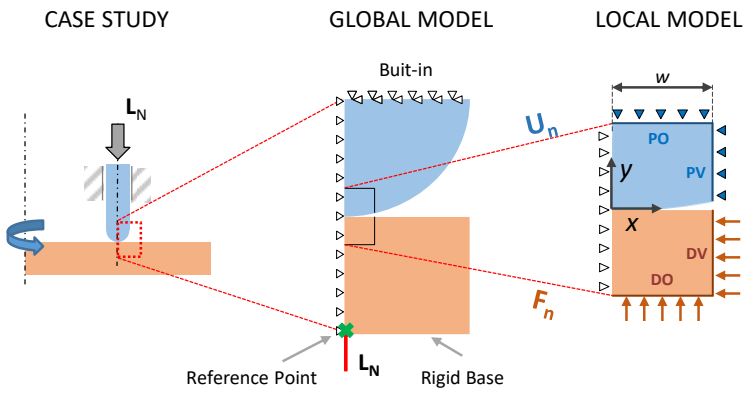

Fig. 1.10. Case study on f pin-on-disc. BCs and geometries of the global and local model. Nodal forces F_n and nodal displacements U_n were extracted from the global model solution and mapped respectively to the disc and pin boundaries (DO, DV, PO and PV). (Adapted and reprinted from [3] with permission from Elsevier).

1.3.2.2 *Results*

a) Convergence analysis of the global model

The global model convergence analysis is a fundamental step of the procedure. As already stressed, the boundary error on the quantities to be transferred to the local model must be minimized by properly selecting the mesh density. Fig. 1.11 shows some results on the influence of the edge element size (h_G) near the contact on the nodal displacement profiles at the DO and DV boundaries defined in Fig. 1.10. Slightly different solutions were obtained varying the element size with discrepancies that were reduced with the mesh refinement. The 'right enough' mesh size should be obviously defined based on the acceptable convergence criteria for the desired solution accuracy. In this case, a coarse mesh with h_G=1/3a was selected because percentage differences on both displacement and nodal stresses at the cut boundaries were always lower than 1%.

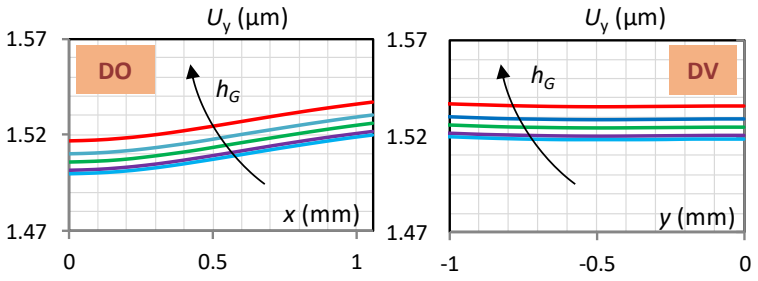

Fig. 1.11. Variation of the displacements U_y profiles along the cut boundaries DO and DV with a decreasing value of the element edge size (h_G) near the contact region of the global model. (Adapted and reprinted from [3] with permission from Elsevier).

b) Definition of the cut boundaries

The size of the subregions was selected based on two opposite requirements: a small value of w to reduce the computational cost and a large value of w to guarantee that, at the end of test, the cut boundaries were still far enough away from the stress concentration region. A value of w=1 mm proved to be a good compromise: in the final worn configuration, the contact area increased up to five times its initial value

and the half contact width reached a value of about *w*/2. The fact that the cut boundaries were properly chosen was demonstrated by the procedure validation results that will be discussed in the following. In particular, it was demonstrated that the BCs extracted at the selected interfaces did not vary significantly with wear. As an example, Fig. 1.12 shows the variation of the nodal stress distribution at the DO and DV with the sliding distance *d* obtained simulating the wear test with the entire global model. A maximum percentage difference on normal stresses of about 20% (the variation of the displacement field was less marked) proved to have an insignificant effect on the wear results.

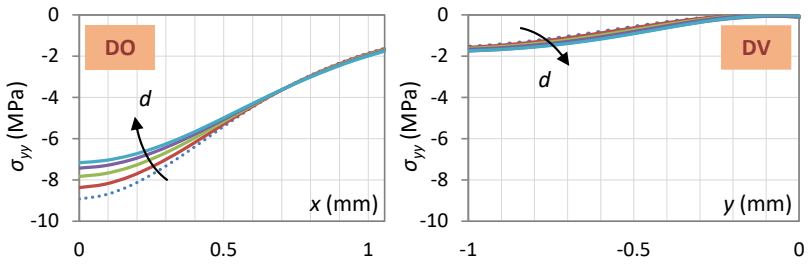

Fig. 1.12. Trend of the stresses σ_{yy} along the DO and DV boundaries during the wear simulation performed with the global model. (Reprinted from [3] with permission from Elsevier).

c) Definition of the boundary conditions

Among the different boundary condition configurations tested, the hybrid approach where nodal forces and displacements were combined and applied on the local model interfaces (Fig. 1.10) proved to be the most efficient solution. This strategy helps preventing numerical issues due to displacement constraints and; on the other hand, the nodal force constraint ensures contact between the two bodies during the entire wear simulations.

d) Convergence analysis of the local model

The mesh size of the local model was selected based on a typical mesh convergence analysis aimed at reducing the discretization error on the maximum contact pressure in the initial unworn configuration. An element

edge size of about h_L=a/10 at the contact region was considered acceptable to accurately predict both contact pressure and wear from the first wear cycles. However, interesting results regarding the effect of mesh size on the accuracy of the wear estimation demonstrated that wear computation is less sensitive to the discretization error when the contact pressure profile flattens due to the volume loss and the contact became more conformal. In this case, a coarse mesh model (i.e., h_L=a/2), that roughly predict wear and stresses in the initial phase, proved to be enough to estimate volume loss at the end of the test with a good level of accuracy. In Fig. 1.13, the trend of the relative percentage errors on the volume lost (e_A) between the numerical and the theoretical Archard solution as the sliding distance d increases, is presented for both fine and coarse local models. It can be noted that this quantity decreased markedly with d and an error of about 10% at the beginning can be reduced to 1% after about d=600 m for the coarse mesh model. A significant reduction of the computational time was observed: the FE wear analysis performed with the coarse mesh model took almost 1/3 of the time needed by the fine mesh model to complete the simulation. The compromise between high predictive accuracy and low computational cost should be thus evaluated also based on the specific phase of interest of the wear test.

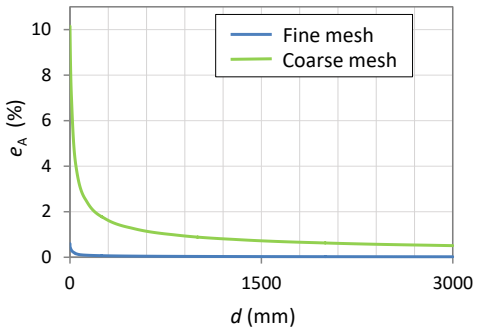

Fig. 1.13. Trend of the relative percentage errors on the volume lost (e_A) between the numerical and the theoretical Archard solution as the sliding distance d increases for both fine and coarse mesh local models. (Adapted and reprinted from [3] with permission from Elsevier).

e) Wear results and procedure validation

The main contact and wear results obtained with the local model are shown in Fig. 1.14. Typical trends of the maximum contact pressure (P_{max}), maximum wear depth (h_{max}) and wear volume with increasing values of the travelled distance d can be observed (Fig. 1.14(b, d)). As the wear proceeded the contact became more conformal due to the volume loss on the pin surface and the contact profile rapidly flattened, as also demonstrated by the evolution of contact pressure and pin wear profiles (Fig. 1.14(a, c)). A first running-in phase where the maximum contact pressure drastically decreased and the value of the maximum wear increased rapidly and nonlinearly is followed by a quasi-steady state condition characterized by a linear increase of h_{max} and an almost constant value of P_{max}. These results were in fully agreement with the experimental and numerical study reported in [12] and, more importantly in the context of procedure validation, they were almost identical (discrepancies lower than 0.5%) to the ones obtained simulating the same wear test with the global model. A significant reduction of the computational time was observed using submodeling wear procedure: to reach the same level of accuracy, the global model took more than twice the time needed for the local wear model to complete the simulation.

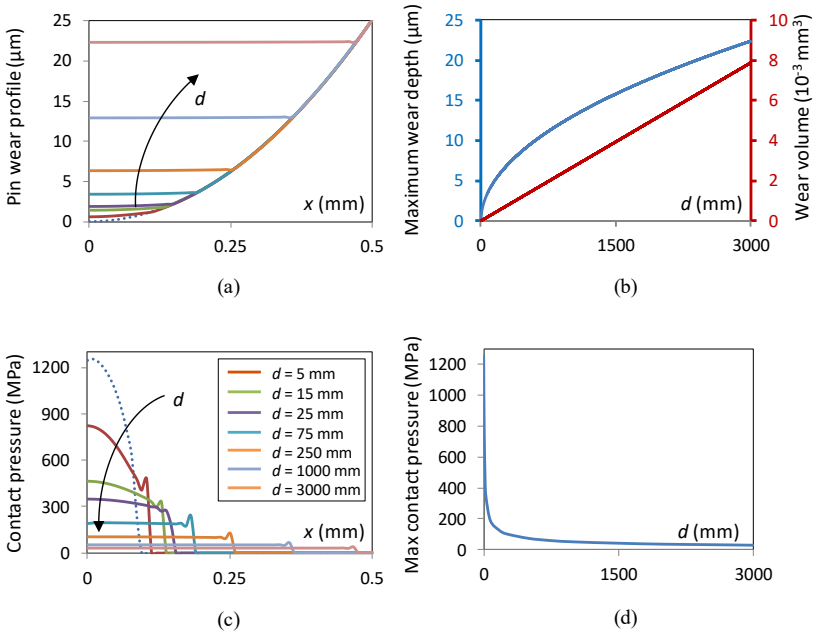

Fig. 1.14. Main contact and wear results obtained with the local model in term of (a) pin wear profile, (b) maximum wear depth and wear volume, (c) contact pressure profile and (d) maximum contact pressure evolution with the sliding distance *d*. Contact pressure and wear profiles before wear are plotted with dashed lines. (Adapted and reprinted from [3] with permission from Elsevier).

1.4 Conclusions

FE modeling allows to fully predict the contact conditions in presence of wear capturing the geometrical changes and the contact pressure evolution, aspects not considered in analytical wear simulations. However, that typically implies high computational costs that can be reduced adopting one or a combination of computational strategies, depending on the simulated case. In particular, in this Chapter, the accelerated wear procedure and the submodeling technique are presented and discussed in

details for simple case studies, demonstrating their ability to reduce the simulation duration. However, in order to obtain reliable results, the procedure parameters (e.g. $\overline{N}$ or the cut boundaries geometry) must be set carefully, by means of ad hoc sensitivity analyses. Moreover, as for the analytical wear models, the FE wear model validity should be assessed considering both wear volume and wear map.

1.5 References

[1] J. Lengiewicz, S. Stupkiewicz, Efficient model of evolution of wear in quasi-steady-state sliding contacts, Wear, 303 (2013) 611-621.
[2] I.R. McColl, J. Ding, S.B. Leen, Finite element simulation and experimental validation of fretting wear, Wear, 256 (2004) 1114-1127.
[3] C. Curreli, F. Di Puccio, L. Mattei, Application of the finite element submodeling technique in a single point contact and wear problem, International Journal for Numerical Methods in Engineering, 116 (2018) 708-722.
[4] L. Mattei, F. Di Puccio, Influence of the wear partition factor on wear evolution modelling of sliding surfaces, Int J Mech Sci, 99 (2015) 72-88.
[5] C. Mary, S. Fouvry, Numerical prediction of fretting contact durability using energy wear approach: optimisation of finite-element model, Wear, 263 (2007) 444-450.
[6] L. Johansson, Numerical simulation of contact pressure evolution in fretting, J Tribol, 116 (1994) 247-254.
[7] N. Stromberg, An augmented Lagrangian method for fretting problems, European Journal of Mechanics, A/Solids, 16 (1997) 573-593.
[8] L. Rodríguez-Tembleque, R. Abascal, M.H. Aliabadi, A boundary element formulation for wear modeling on 3D contact and rolling-contact problems, International Journal of Solids and Structures, 47 (2010) 2600-2612.
[9] S. Mukras, N.H. Kim, W.G. Sawyer, D.B. Jackson, L.W. Bergquist, Numerical integration schemes and parallel computation for wear prediction using finite element method, Wear, 266 (2009) 822-831.
[10] N.H. Kim, D. Won, D. Burris, B. Holtkamp, G.R. Gessel, P. Swanson, W.G. Sawyer, Finite element analysis and experiments of metal/metal wear in oscillatory contacts, Wear, 258 (2005) 1787-1793.
[11] N.G. Cormier, B.S. Smallwood, G.B. Sinclair, G. Meda, Aggressive submodelling of stress concentrations, International Journal for Numerical Methods in Engineering, 46 (1999) 889-909.

[12] P. Põdra, S. Andersson, Simulating sliding wear with finite element method, Tribol Int, 32 (1999) 71-81.